Updraft and Downdraft Cores in TOGA COARE: Why So Many Buoyant Downdraft Cores?

RICHARD C. IGAU*

Texas A&M University, College Station, Texas, and
National Center for Atmospheric Research,+ Boulder, Colorado

MARGARET A. LEMONE

National Center for Atmospheric Research,+ Boulder, Colorado

DINGYING WEI#

Department of Physics and Geophysical Research Center, New Mexico Institute of Mining and Technology, Socorro, New Mexico

(Manuscript received 16 March 1998, in final form 4 September 1998)

ABSTRACT

An examination of the properties of updraft and downdraft cores using Electra data from TOGA COARE shows that they have diameters and vertical velocities similar to cores observed over other parts of the tropical and subtropical oceans. As in previous studies, a core is defined as having vertical velocity of the same sign and greater than an absolute value of 1 m s^{-1} for at least 500 m. A requirement that the core contain either cloud or precipitation throughout is added, but this should not affect the results significantly.

Since the Electra was equipped with the Ophir III radiometric temperature sensor, it was also possible to make estimates of core buoyancies. As in TAMEX and EMEX, where core temperatures were estimated using the modified side-looking Barnes radiometer on the NOAA P3s, a significant fraction of both updraft and downdraft cores had apparent virtual temperatures greater than their environments. In fact, the average virtual temperature deviation from the environment for downdraft cores was +0.4 K.

Sixteen of the strongest downdraft cores were examined, all of which had positive virtual-temperature deviations, to find the source of this surprising result. It is concluded that the downdraft cores are artificially warm because 100% relative humidity was assumed in calculating virtual temperature. However, reducing core mixing ratios to more physically realistic values does not eliminate warm virtual potential temperature downdraft cores, nor does water loading make all cores negatively buoyant. Thus positively buoyant convective downdrafts do exist, though probably in smaller numbers than previously suggested.

1. Introduction

Oceanic convective cores sampled in the Global Atmospheric Research Program (GARP) Atlantic Tropical Experiment (GATE) were compared to continental cores by LeMone and Zipser (1980) and Zipser and LeMone (1980), who defined a convective core as having vertical velocity of the same sign and greater than an absolute value of 1 m s^{-1} for at least 500 m. They found that the oceanic cores were weaker and smaller than continental cores sampled during the Thunderstorm Project (Byers and Braham 1949) over Florida and Ohio. Since then, similar studies were repeated for mature hurricanes (Jorgensen et al. 1985), the subtropical Pacific [Taiwan Area Mesoscale Experiment (TAMEX); Jorgensen and LeMone 1989], and the Tropics north of Australia [Equatorial Mesoscale Experiment (EMEX); Lucas et al. 1994], with similar results.

More recently, Jorgensen and LeMone (1989), Lucas et al. (1994), and Wei et al. (1998) have used radiometric temperature measurements to estimate convective-core virtual temperatures. The apparent abundance of downdraft cores with virtual temperatures higher than the environment was surprising. Jorgensen and LeMone (1989) and Lucas et al. (1994) suggested that water loading compensated to make the downdraft cores neg-

* Current affiliation: El Paso Energy Marketing Company, Houston, Texas.

+ The National Center for Atmospheric Research is sponsored by the National Science Foundation.

Current affiliation: University Advancement, University of California, Irvine, Irvine, California.

Corresponding author address: Margaret A. LeMone, NCAR, P.O. Box 3000, Boulder, CO 80307.
E-mail: lemone@ucar.edu

atively buoyant. However, using data taken in the equatorial Pacific during the Tropical Ocean Global Atmosphere Coupled Ocean–Atmosphere Response Experiment (TOGA COARE), Wei et al. (1998) found that the liquid-water contents in downdraft cores were not sufficient to provide negative or even neutral buoyancy.

In this paper, we compare the characteristics of convective cores sampled during TOGA COARE (Webster and Lukas 1992) to previous observations and explore the buoyancy issue further by taking a closer look at the strongest downdraft cores, which all had virtual temperatures warmer than their environments.

After describing sampling and data analysis in section 2, we establish in section 3 that the COARE convective cores have sizes and vertical velocities similar to cores sampled over other parts of the tropical and subtropical oceans, except that the updraft cores have slightly lower virtual temperatures and the downdraft cores appear to have higher virtual temperatures, relative to the environment. In section 4, we examine 16 of the strongest downdraft cores to explore what makes the downdraft-core virtual temperatures so high in COARE, including the differences between the Ophir instrument and earlier radiometric measurements, the assumption of 100% relative humidity in calculating core virtual temperature, height differences typical of downdraft penetrations, and water loading. We conclude that the assumption of water vapor saturation in cores, used in core studies for lack of better information, conspires with the Ophir radiometer's more accurate (warmer) temperature estimate in rain to make the COARE downdraft cores appear to have higher virtual temperatures relative to the environment than those sampled in TAMEX and EMEX. We also conclude that the saturation assumption has led to overestimates of virtual temperatures in downdraft cores for all three experiments. However, after estimating minimum reasonable buoyancies for the strongest downdraft cores and examining downdraft behavior in some numerical simulations of deep convection in the Tropics, we suggest that positively buoyant downdraft cores are fairly common.

2. Data

a. Data collection methods

The data used in this study were collected by the National Center for Atmospheric Research (NCAR) Electra during TOGA COARE, in a variety of convection, ranging from isolated towering cumulus to groups or clusters of precipitating clouds that had both growing and decaying elements, to active squall lines. Several aircraft penetrated precipitating convection between 30 m and 6 km above mean sea level (msl), including two P3s from the National Oceanic and Atmospheric Administration (NOAA), a C-130 operated by the U.K. Meteorological Research Flight, and an Electra operated by NCAR. We restrict ourselves to the Electra because it was instrumented with an Ophir instrument believed to have unprecedented success at measuring temperature in cloud (Cooper 1987; Lawson and Cooper 1990). Fortunately, the Electra also provided the best sample of convective cores below 6 km. The P3 flight patterns were primarily flown to optimize use of their Doppler radars, resulting in few penetrations until late in a convective system's life cycle. This left the Electra, which was without a Doppler radar for the first half of the experiment, as the primary penetration aircraft. During the second half of the experiment, even with its Doppler radar aboard, the Electra performed more penetrations than did the P3s, both in coordinated patterns and in single-aircraft missions. Since the emphasis was on the mesoscale, the Electra did not usually target convective towers. The Electra typically flew at a constant altitude near 700 mb (approximately 3 km) so the data presented here are concentrated near this level.

Historically, temperatures and dew points from aircraft were measured using immersion techniques, which involve direct contact of the sensor with the air. However, there is overwhelming evidence that sensor wetting leads to temperatures that are too low in warm clouds, that is, those with temperatures above -2°C (Lenschow and Pennell 1974; Heymsfield et al. 1979; LeMone 1980; Cooper 1987; Lawson and Rodi 1987; Blyth et al. 1988; Lawson and Cooper 1990), and dew points that are too high (e.g., Zipser et al. 1981). Moreover, it is impossible to correct for either effect since it is difficult to determine how much of the sensor is wet.

In principle, radiometric techniques should work better. Indeed, there is evidence that airborne radiometric thermometers can make better temperature measurements in warm clouds. The first such measurements showed that in-cloud sensible heat fluxes from radiometric data were more than four times greater than those derived from Rosemount measurements, and they were in good agreement with the results from a numerical simulation (Albrecht et al. 1979). Jorgensen and LeMone (1989) used data from a radiometric temperature sensor to show that the relationship of updraft-core buoyancy and the vertical variation of vertical velocity was consistent with parcel theory. Cooper (1987) concluded that the temperature measured by a carefully calibrated Ophir radiometer agreed well with the temperature measured by immersed sensors in clear air and that the Ophir was not affected by wetting inside clouds.

The Ophir III radiometric thermometer was used in TOGA COARE. It senses the spectral radiance at a wavelength of 4.25 μm rather than at 15 μm as done previously using a side-looking Barnes radiometer mounted on the NOAA P3 aircraft (Albrecht et al. 1979; Jorgensen and LeMone 1989; Lucas et al. 1994). Carbon dioxide is a stronger absorber and emitter at 4.25 μm than at 15 μm so the sample volume of the Ophir is smaller and located closer to the aircraft. If we define sample path length by the distance from which 90% of the signal is received, the sample path length is 10 m

for the Ophir radiometer and 100 m for the Barnes radiometer (Lawson and Cooper 1990). Thus, steep turns will affect the apparent temperature from the Barnes instrument, which is rigidly mounted to the fuselage. Moreover, both the absorption and the emission by water at 4.25 μm are weaker than at 15 μm. Thus, a 4.25-μm thermometer detects significant radiation from cloud droplets only in very dense clouds, where the difference between the droplet temperature and air temperature is believed to be smaller than 0.1 K (Lawson and Cooper 1990). On the other hand, temperature measurements made by a radiation thermometer measuring at 15 μm can be too low in subsaturated rainshafts where drops will have temperatures close to the wet-bulb temperature.

b. Processing of the Ophir temperature data

During TOGA COARE, the Ophir had three problems that made careful processing necessary: an offset and long-term drift, fluctuations too large in amplitude, and intermittent 1–2-s spikes. The Ophir data used here were processed by Wei et al. (1998), who use the temperature measured by the Rosemount probe (T_{ros}) in clear air as a baseline for the Ophir data. The procedure involves the following six steps.

1) Remove the water-induced cooling signal from the reference temperature T_{ros} by linearly interpolating T_{ros} between points 20 s before and 20 s after each cloud or rain penetration. Based on careful examination of the data, rain or cloud penetrations coincide with forward scattering spectrometer probe (FSSP) cloud liquid-water content greater than 0.03 g m^{-3}. According to Wei et al. (1998) this approach works well unless the aircraft is inside cloud too long.
2) Obtain the high-frequency part of the raw Ophir temperature, T_{oat}, signal by subtracting out the low-passed T_{oat} data obtained using a filter with a cutoff frequency of 1.59×10^{-3} Hz (approximately 60 km for an aircraft traveling at 100 m s^{-1}).
3) Despike T_{oat} by linearly interpolating through spikes that exceed an empirically determined threshold of 0.8 K.
4) Multiply the high-frequency fluctuations thus obtained by a scale factor determined by comparing the high-frequency Ophir and Rosemount data in clear air.
5) Low-pass filter T_{ros} using the same filter.
6) Add the Ophir and Rosemount temperature signals processed in steps 1–5 to obtain the corrected temperature T_{cor}.

Figure 1, a cloud penetration from 19 November 1992, compares the performance of the corrected Ophir temperature T_{cor} to T_{ros} and the temperature from a reverse-flow thermometer. The wetting effect on the immersion sensors is shown clearly. Both Rosemount and reverse-flow temperature signals drop significantly upon entering the cloud and require about 10 s to dry after exiting the cloud. The Ophir probe shows less cooling than T_{ros} or the reverse-flow temperature in the first cloud, which had downward motion and low liquid water. The Ophir shows warming in the second cloud, which has a higher liquid-water content. Here T_{cor} agrees well with T_{ros} outside of cloud except for the T_{ros} drying-out period after penetrations.

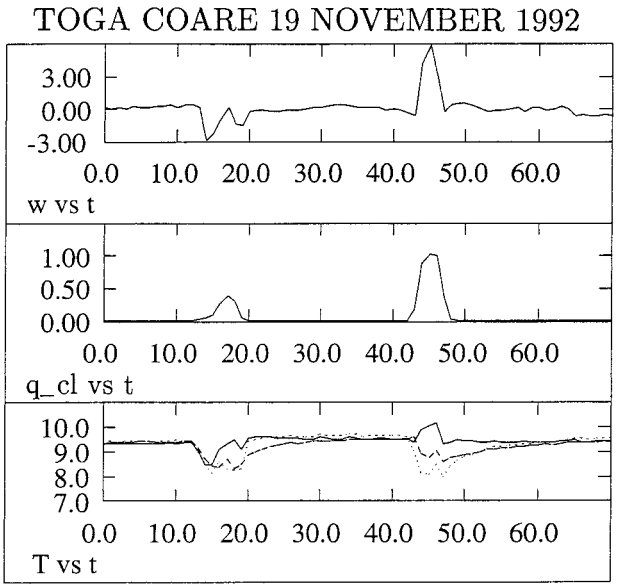

FIG. 1. Data from a cloud penetration (1759:20–1800:30 UTC) on 19 November 1992. From top to bottom: vertical air velocity (w) in m s^{-1}, cloud liquid water content (q_{cl}) in g m^{-3}, and temperature measurements (T), from two immersion sensors, the Rosemount (T_{ros}, dashed line) and the reverse flow (dotted line), and the corrected Ophir temperature (T_{cor}, solid line). Figure from Wei et al. (1998).

Figure 1 shows that the corrected Ophir temperature T_{cor} can be greater in cloud than in the clear-air region, as expected from parcel theory. Since we have thermodynamic measurements below cloud base and in environmental aircraft soundings, we can estimate the possible range of temperatures for a parcel rising from cloud base. For a typical day, Fig. 2 compares T_{cor} sampled in cloud to the highest possible (adiabatic) temperature and the lowest possible temperature, obtained by mixing the parcel with the environment at constant pressure and evaporating all the condensed water until saturation. Clearly, T_{cor} lies between the allowable extremes for such a parcel. This is true for all cases examined, even though such a calculation does not allow for penetrative downdrafts.

c. Analysis

The unfiltered 1-Hz vertical velocity from the Electra gust probe and measures of cloud and precipitation water are used to identify updraft and downdraft ''cores.'' As in LeMone and Zipser (1980) and subsequent studies, a core is defined as a region of upward or downward

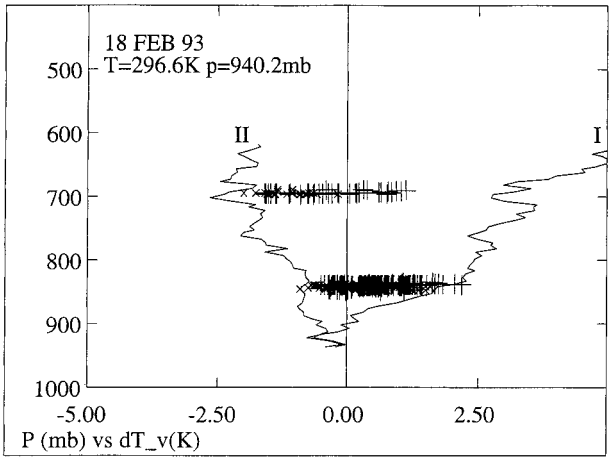

FIG. 2. The vertical profile of virtual temperature excess for a moist air parcel from cloud base (T = 296.6 K and p = 940.2 mb) from (I) adiabatic process and (II) mixing the cloudy air with the environmental air and evaporating condensed water until saturation is reached. The measurements in cloud regions with no particles larger than 800 μm: + signs for $w > 1$ m s^{-1}; × for $w < -1$ m s^{-1}. From Wei et al. (1998), to which the reader is referred for details.

air motion equaling or exceeding 1 m s^{-1} for at least a 500-m distance. Only cores sampled on straight and level legs are included. Each core is required to be within cloud or precipitation. While such a criterion was not applied in previous studies, it probably does not have a significant effect, since updraft and downdraft cores are rare in clear air at the altitudes examined. A core is considered to be within cloud or precipitation if any one of three criteria is satisfied for all 1-s measurements within the core, namely, 1) concentration of cloud particles measured by the Particle Measuring Systems (PMS) 2D-C probe exceeds 0.1 L^{-1}, 2) the concentration of particles measured by the PMS 2D-P probe exceeds 0.1 L^{-1}, or 3) the King probe liquid-water content exceeds 0.2 g m^{-3}. The thresholds are based on examining and comparing videos and time series; the 0.2 g m^{-3} value was selected because lower values often reflected noise or offsets in the data. Our criteria for identifying regions of cloud and rain are somewhat different from those of Wei et al. (1998), but this should not affect our results.

Buoyancy estimates require information about the cloud-free environmental conditions near the cores. The environment is required to be in dry air (fail the cloud test) and is computed from the average of two 60-s periods beginning 90 s before and 30 s after the aircraft encounters the cloudy region containing the core(s). This requires a period of 150 s (roughly 15 km) of cloud-free air between cloud penetrations for a region to qualify as ''environment.'' The 30-s delay period surrounding the cloud is an attempt to avoid any detrained cloud material that might have evaporated and moistened the region near the cloud and to avoid problems due to instrument drying. Both of the environmental regions are tested to assure that the altitude of the aircraft did not vary by more that 100 m within each 60-s period and that the average altitudes are within 100 m of the average altitude of the core. If one of the ''before'' or ''after'' environmental regions fails either of these tests, then only the ''good'' time period is used for the environmental calculations. If both regions fail the test, then the core is not used in the analysis. In the worst-case scenario, the average altitude of the two environmental regions would be 200 m apart, but this did not happen. The average altitudes of only 11 updraft cores (6% of the sample) and 6 downdraft cores (4%) differed from the average altitude of the environment sample by more than 30 m.

Several characteristics of the cores are computed. These include the average and maximum vertical-velocity (w) deviations; the average and maximum particle concentrations measured by the PMS 2D-C, 2D-P, and FSSPs processed by NCAR; the virtual-temperature (T_v) deviations between the core and the environment; and the intercepted length of the core (D), referred to loosely as the core ''diameter.'' Virtual temperature is defined in the conventional way, that is, $T_v = T(1 + 0.61q)$, where T is temperature (K) and the mixing ratio q is dimensionless. In the environment, the mixing ratio is derived from the General Eastern Model 1011B dewpoint hygrometer, which registers saturation when water or ice forms on a chilled mirror. This instrument, similar to that used for the measurements in Zipser et al. (1981), fails in warm clouds or precipitation. Thus q in cores is specified assuming saturation, as in previous studies. The diameter is calculated by multiplying the true air speed of the aircraft inside the core by the duration of the core. The maximum deviations for T_v and w are defined as the most positive for updraft cores and the most negative (or least positive) for downdraft cores. For simplicity, we will use the words ''warmer'' and ''cooler'' when referring to virtual temperature and temperature deviations.

The particle-concentration data from the 2D-C and 2D-P optical-array probes are used for statistical comparisons for all the data (section 3) and for computing the contribution of water loading to buoyancy for strong downdraft cores (section 4). The ''raw'' data are used for the statistics. However, the liquid-water contents are found by Wei et al. (1998) by integrating the masses of all the particles sampled by the 2D-P and 2D-C probes after removal of artifacts, and accounting for the effects of canting and nonspherical shapes of the 2-D images.

The Electra vertical velocity w is basically calculated as described in Lenschow (1972).[1] Estimated absolute accuracy is ~1 m s^{-1} (Lenschow 1972), but the deviations from the mean have an uncertainty of only 0.1

[1] For an up-to-date description of the calculations, see Research Aviation Bulletin 23, Measurement Techniques: Air Motion Sensing, by Lenschow and Spyers-Duran.

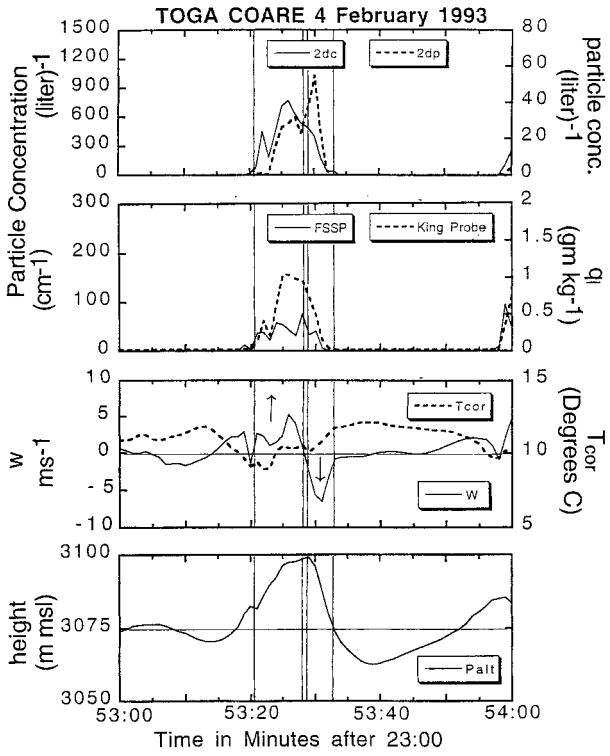

FIG. 3. For 4 February 1993, updraft and downdraft core (core 10 of Fig. 9), in cumulus congestus, at about 3.1 km: (top frame) particle counts per liter for PMS 2D-C probe (drop diameter d = 25–800 μm) and 2D-P probe (d = 200–6400 μm); King Probe (second frame) particle count from the PMS FSSP probe (d = 3–45 μm) and liquid-water content; (third frame) Ophir temperature T_{cor} produced by Wei et al. (1998) and vertical velocity w; (bottom frame), pressure altitude. Cores are designated by vertical lines. For all the frames, the left scale applies to the solid lines and the right scale applies to the dashed lines.

m s^{-1} (Lucas et al. 1994). Thus the leg-average vertical velocity was subtracted from the 1-s measurements for that leg. This adjusts the leg-average vertical velocity to zero, as done in the previous core studies. The corrections, typically 0.2 m s^{-1} or less, were of the order of the uncertainty of the relative measurements.

Legs are defined as being at near-constant altitude and determined objectively using an algorithm that identifies changes in altitude. Since the aircraft did not change altitudes very often, most constant altitude legs (turns included) are over 360 km in length, with some ferry legs extending over 1000 km. Cores sampled in turns were subsequently removed from the sample.

Figure 3 illustrates penetrations of an updraft and downdraft core associated with a relatively isolated cumulus congestus ahead of a convective band. Both contain liquid water in the form of cloud droplets (high FSSP particle count) and raindrops (high 2D-P count), but the downdraft has more large drops (higher 2D-P count). In this particular case, the Ophir temperature T_{cor} signal shows a cloud cooler than its local environment. The video shows the penetration is near the top of the cloud, suggesting that Fig. 3 shows an overshooting cloud top.

Updraft and downdraft cores were sampled at various levels on 23 of the 32 Electra missions during TOGA COARE. Table 1 gives the distribution of cores by flight and by altitude. The altitude intervals, chosen to match those of other investigators are 0–0.7 km, 0.7–2.5 km, 2.5–4.3 km, 4.3–5.8 km, and greater than 5.8 km. Research fight 25 is not included in the analysis due to problems calculating T_{cor} on that flight. The majority of the updraft and downdraft cores were sampled near 3 km and come primarily from eight flights in and near organized convection. These flights sampled small linear bands of convection and large mesoscale convective systems from which 185 updraft cores and 147 downdraft cores were identified. The measurements were taken in both convective and stratiform regions of these systems. Because so few cores were sampled at the other height intervals we restrict ourselves to these cores in subsequent discussion unless otherwise indicated.

3. Results

The updraft and downdraft cores sampled by the Electra in TOGA COARE are similar to those reported in other tropical oceanic regions of the world, and smaller and much weaker than the midlatitude continental cores reported in the Thunderstorm Project and other studies (e.g., Heymsfield and Hjelmfelt 1981; Musil et al. 1986). Table 2 lists the median, the range of values, and the strongest 10%[2] value of mean w, maximum 1-s w deviation (w_{xtrm}), and diameter (D) from TOGA COARE. Figures 4a–c compare these characteristics with observations of oceanic cores in EMEX (Lucas et al. 1994), TAMEX (Jorgensen and LeMone 1989), GATE (LeMone and Zipser 1980), hurricane rainbands (Jorgensen et al. 1985), and continental cores in the Thunderstorm Project (Byers and Braham 1949). Only the data from the 2.5–4.3-km height interval are plotted in the diagrams and almost all the cores are from ~3 km msl. The 10% values for the average vertical velocity, extreme 1-s vertical velocity, and core diameter are all similar to the values reported from the other oceanic studies.

Assuming similar entrainment, it is not surprising that the vertical velocities in COARE are similar to those from GATE, EMEX, and hurricane rainbands. The buoyancy in all four cases is modest (less than 4–5 K) and spread fairly evenly through the troposphere, in contrast to the Thunderstorm Project soundings, which showed larger buoyancies at low levels (Lucas et al. 1994). Consistent with this, the average convective available potential energy integrated to 500 mb using

[2] A 10% value here is taken as being greater than or equal to 90% of the values in the sample.

TABLE 1. Distribution of convective updraft and downdraft cores by flight date and altitude, for the NCAR Electra in TOGA COARE. Heights in kilometers.

Mission		Updraft cores by height interval*					Downdraft cores by height interval					
Flight no.	Date	<0.7	0.7–2.5	2.5–4.3	4.3–5.8	5.8+	<0.7	0.7–2.5	2.5–4.3	4.35–5.8	5.8+	Remarks
1	15 Nov 1992	—	—	—	—	1	—	—	—	—	1	
2	19 Nov 1992	—	—	23	—	—	—	—	13	3	—	
3	16 Nov 1992	—	—	—	3	—	—	—	—	2	—	
4	28 Nov 1992	—	—	—	—	—	—	—	—	—	—	No cloud penetrations
5	02 Dec 1992	—	—	—	—	—	—	—	—	—	—	No cloud penetrations
6	03 Dec 1992	—	1	—	1	—	—	—	—	—	—	
7	04 Dec 1992	1	9	—	2	—	2	3	—	—	—	
8	06 Dec 1992	1	3	—	—	—	2	6	—	—	—	
9	07 Dec 1992	—	—	—	—	—	—	—	—	—	—	No cloud penetrations
10	08 Dec 1992	—	—	—	—	—	—	—	—	—	—	No cloud penetrations
11	09 Dec 1992	—	—	—	—	—	—	—	—	—	—	No cloud penetrations
12	10 Dec 1992	—	—	—	—	—	—	—	1	—	—	
13	13 Dec 1992	—	2	—	4	—	—	—	—	6	—	
14	14 Dec 1992	—	1	29	—	—	—	—	38	—	—	
15	15 Dec 1992	—	—	28	—	—	—	—	15	—	—	
16	16 Dec 1992	—	—	—	1	—	—	—	—	—	—	
17	09 Jan 1993	2	—	—	—	—	—	—	—	—	—	
18	12 Jan 1993	—	—	1	—	—	—	1	—	—	—	
19	13 Jan 1993	—	—	—	—	—	—	—	—	—	—	No cloud penetrations
20	14 Jan 1993	—	—	—	—	—	—	—	—	—	—	No cloud penetrations
21	16 Jan 1993	—	—	—	—	5	1	—	—	—	2	
22	17 Jan 1993	2	—	—	—	—	—	—	—	—	—	
23	18 Jan 1993	1	—	—	—	—	1	—	—	—	—	
24	26 Jan 1993	—	—	—	—	—	—	—	—	—	—	No cloud penetrations
25	27 Jan 1993	—	—	—	—	—	—	—	—	—	—	Data problems
26	28 Jan 1993	—	1	—	7	2	—	—	—	—	1	
27	04 Feb 1993	2	—	14	—	—	2	—	17	—	—	
28	06 Feb 1993	—	—	31	—	—	—	—	6	—	—	
29	09 Feb 1993	—	—	39	—	—	—	—	36	—	—	
30	10 Feb 1993	—	—	12	—	—	—	—	19	—	—	
31	17 Feb 1993	—	2	—	2	—	—	1	—	1	—	
32	18 Feb 1993	3	23	8	1	—	—	15	2	—	—	
	TOTAL	12	42	185	21	8	8	26	147	12	4	

* Altitude intervals strictly defined as 0.7–2.499 km, 2.5–4.299, etc.

the proximity soundings that LeMone et al. (1998) constructed for organized COARE convection (360 ± 66 J kg^{-1}) is not significantly different from the values for fast (377 J kg^{-1}) and slow (379 J kg^{-1}) lines in GATE computed from the data in Barnes and Sieckman (1984).

The distributions of average and 1-s extreme deviation of core virtual temperature T_{vc} from the environment virtual temperature T_{ve} are shown in Fig. 5, for the cores sampled at altitudes between 2.5 and 4.3 km msl. The deviations are found by subtracting the environmental value of T_v from the core value. The extreme deviation represents the warmest 1-s value of T_v for updraft cores but the coolest 1-s T_v value for downdraft cores. Here, T_{ve} is calculated using T_{cor} and the measured mixing ratio in the environment, but saturation is assumed for T_{vc} since the water vapor measurements are erroneous in rain or warm cloud. The assumption of saturation is reasonable for updraft cores since they are likely to be in cloud. For downdraft cores, which may contain precipitation but no cloud, the air may be subsaturated.

As in previous experiments, the distributions in Fig.

TABLE 2. Characteristics of TOGA COARE convective cores (2.5–4.3 km); number of updraft cores = 185; number of downdraft cores = 147.

	Downdraft cores			Updraft cores		
Parameter	Median	10%*	Range	Median	10%	Range
Mean w (m s^{-1})	−1.61	−2.9	−1.10 to −4.46	2.25	4.6	1.12 to 7.83
w_{xtrm} (m s^{-1})	−2.12	−4.2	−1.15 to −6.63	3.5	7.7	1.18 to 12.42
D (km)	0.74	1.62	0.50 to 4.38	0.82	1.88	0.50 to 3.93

* A 10% value is defined as being greater or equal to 90% of the values in the sample.

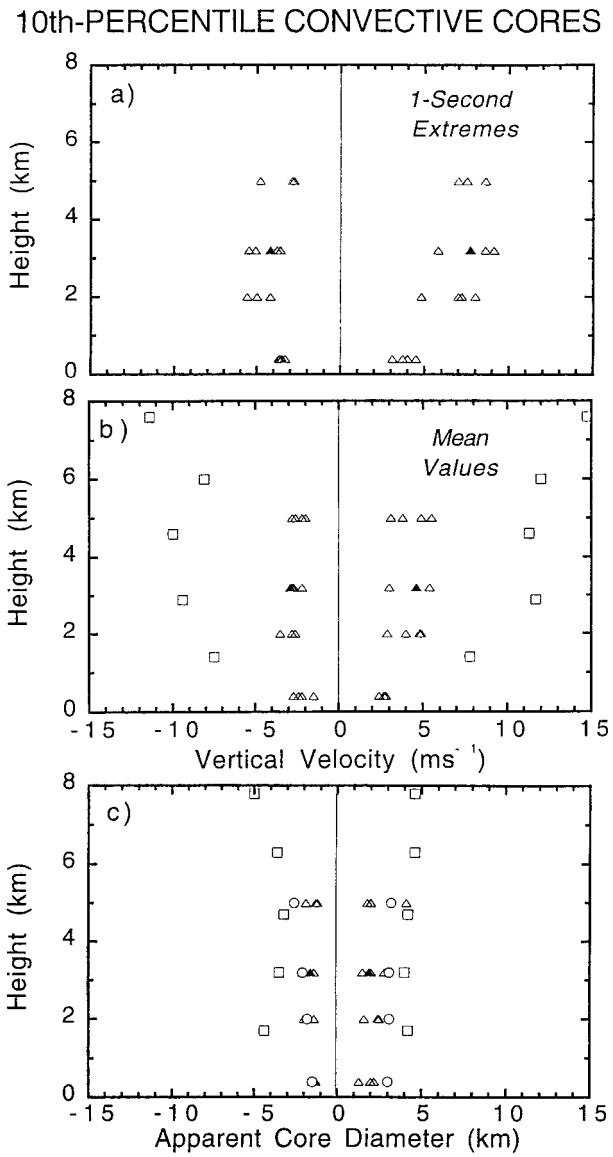

FIG. 4. Comparison of COARE 10% cores (solid triangles) to over-ocean cores sampled during EMEX, GATE, and TAMEX (open triangles); hurricane rainbands (open triangles for vertical velocity, open circles for diameter); and the Thunderstorm Project (squares), for (a) 1-s extreme value of vertical velocity, (b) average vertical velocity, and (c) diameter.

5 show large variation in virtual-temperature deviation for both updraft and downdraft cores. The highest 1-s T_v deviation found in an updraft core was 3.3 C, and the coldest 1-s T_v deviation in a downdraft core was −1.6 C. Because the maximum deviation is defined as positive for updraft cores and negative for downdraft cores, the coldest updraft values and warmest downdraft values are not plotted, but they are worth mentioning. The coldest 1-s T_v deviation in an updraft was −2.4 C, colder than the coldest 1-s value in a downdraft. Similarly, the warmest 1-s T_v deviation in a downdraft was 3.7 C, which is warmer than the warmest 1-s T_v deviation in an updraft.

Table 3 reveals that COARE updraft cores are the coolest relative to their environments for the three experiments and that downdraft cores are the warmest. The average of the mean core T_v deviations for the COARE updraft cores is 0.4 K, lower than for EMEX and TAMEX. Similarly, the 1-s deviations for updraft cores average 0.7°C, slightly cooler than the 1.0°C average from EMEX. For downdraft cores, the average of the mean core T_v deviations is 0.4 K, *the same* as that for the updraft cores and warmer than for TAMEX and EMEX. The average of the extreme 1-s values for downdraft cores, like the mean, is warmer than for EMEX.

While the updraft cores may actually have had smaller positive T_v deviations in COARE than in TAMEX, the differences in downdraft-core T_v deviations might result from differences in the radiometric temperature sensors. The Barnes radiometer used in EMEX and TAMEX, working at 15 μ, is affected by the radiance from liquid. This would decrease the measured temperature in subsaturated downdraft cores where rain is falling, leading to apparently colder, less buoyant, downdraft cores. In such circumstances, the assumption of saturation also leads to a smaller increment to be added to the temperature to obtain virtual temperature, decreasing the buoyancy further, relative to what it would be with the same assumption for the Ophir measurement. We will discuss this further in the next section. Updraft cores, which would tend to have more, smaller drops closer to air temperature, would be less affected.

Figures 6a and 6b are scatterplots relating average T_v deviation to average vertical velocity for updraft and downdraft cores. The positive slope and *y* intercept of the regression line is similar to that of the TAMEX updraft cores (Jorgensen and LeMone 1989). The similarities continue between the two datasets in that vertical velocities less than about 4 m s^{-1} correspond to both positive and negative average T_v deviations, but vertical velocities above this value always have positive average T_v deviations. A similar result occurs for the downdraft cores, with vertical velocities less than approximately −2.4 m s^{-1} always associated with positive average T_v deviations. The large scatter observed in these and subsequent plots is not surprising given differences in water loading, diameter, immediate environment, and time in the core life history.

The linear correlation coefficients of average and maximum 1-s T_v deviation with mean *w*, maximum 1-s *w* deviation, and diameter are displayed in Table 4. Modest relationships are exhibited between average and maximum 1-s vertical velocity, and the average and maximum 1-s T_v deviation for updraft cores; but there is almost no relationship between the same quantities for downdraft cores and almost no relationship between average and maximum T_v deviation and core diameter.

The relationship of vertical velocity to virtual-temperature deviation varies slightly among the different

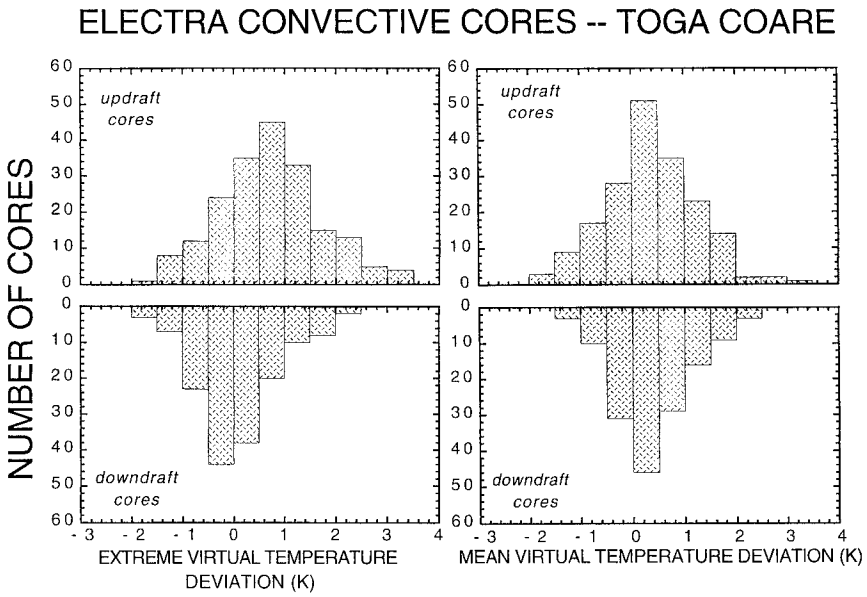

FIG. 5. Distribution of mean and extreme virtual temperature deviations $T_{vc} - T_{ve}$ for updraft and downdraft cores sampled between 2.5 and 4.3 km msl. For the extreme deviations, T_{vc} is the warmest 1-s value in updraft cores and the coldest 1-s value in downdraft cores; for the means, the average core virtual temperature is used. T_{vc} is computed assuming water vapor saturation.

field projects. The linear correlation coefficient between average w and T_v deviation in updraft cores was 0.39 in TAMEX (Jorgensen and LeMone 1989) and 0.54 for TOGA COARE. The linear correlation between average w and average Θ_v deviation was 0.65 in EMEX (Lucas et al. 1994). For downdraft cores, the correlations between average w and average T_v deviations are 0.53 for TAMEX and 0.13 for TOGA COARE; and the correlation between average w and average Θ_v deviation is 0.31 for EMEX.

Average particle counts from the 2D-C (particle diameter 25–800 μm) and 2D-P (particle diameter 200–6400 μm) are plotted against average vertical velocity for updraft and downdraft cores in Figs. 7 and 8, respectively. The strongest updraft cores tend to have the largest numbers of particles in both size ranges and with the higher correlation for the smaller particles. From Fig. 6, strong updraft cores also tend to have larger virtual-temperature excesses.

The number of particles in downdraft cores (Fig. 8) increases with w magnitude. Not surprisingly, the correlation between large drops (2D-P) and vertical velocity is larger for downdraft cores than updraft cores, although the number of drops is smaller for downdraft cores. It is reasonable to ask whether water loading accounts for the relatively warm downdraft cores of Fig. 5, as suggested by Jorgensen and LeMone (1989) and Lucas et al. (1994), or is relatively unimportant, as found in Wei et al. (1998). We deal with this issue in the following section.

4. Discussion

From the foregoing, TOGA COARE is the third field project conducted over the tropical or subtropical oceans for which warm downdraft cores have been observed, and the COARE cores are warmer than those of TAMEX and EMEX. Figure 6 shows that the strongest downdraft cores also have positive virtual-temperature deviations (lower-right quadrant), a relationship also seen in Jorgensen and LeMone (1989, Fig. 8).

We explore these surprising results by examining 16 of the strongest COARE downdraft cores individually. Their characteristics are summarized in Fig. 9. We convert all components of buoyancy to temperature units for more direct comparison; thus, liquid water content (gm m^{-3}) is converted to temperature units by first dividing by air density and then multiplying by core vir-

TABLE 3. Virtual-temperature deviations for convective updraft and downdraft cores (TOGA COARE cores 2.5–4.3 km).

	Updraft cores		Downdraft cores	
	Mean (K)	1-s extreme (K)	Mean (K)	1-s extreme (K)
COARE	+0.4	+0.7	+0.4	−0.1
EMEX (Lucas et al. 1994)	0.6	1.0	0.2	−0.4
TAMEX (Jorgensen and LeMone 1989)	0.7		0.2	

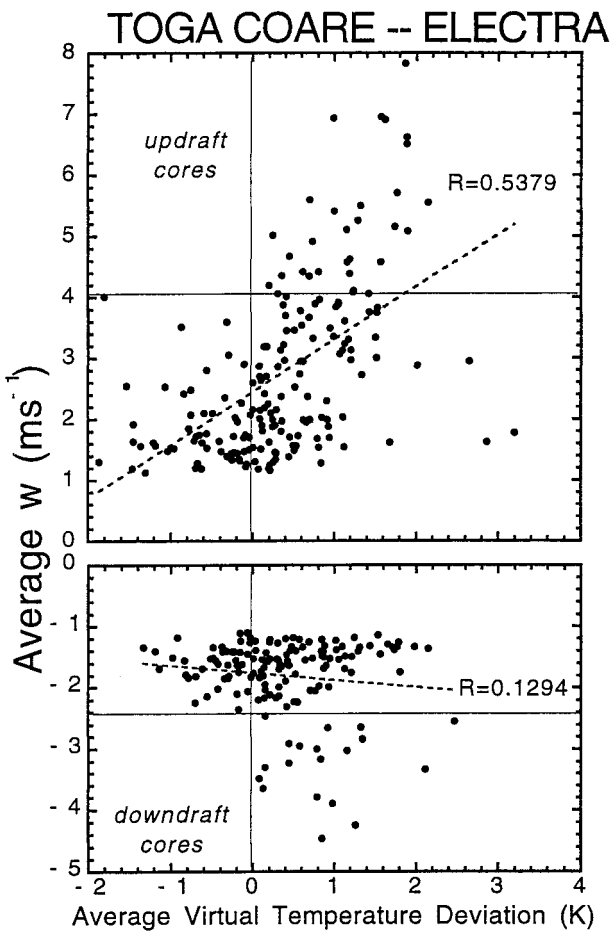

FIG. 6. Average virtual-temperature (T_v) deviation for updrafts and downdrafts vs mean vertical velocity, for updraft and downdraft cores sampled between 2.5 and 4.3 km. Note that all updraft cores with vertical velocities greater than about 4 m s^{-1} and all downdraft cores with vertical velocities less than about -2.4 m s^{-1} have positive T_v deviations.

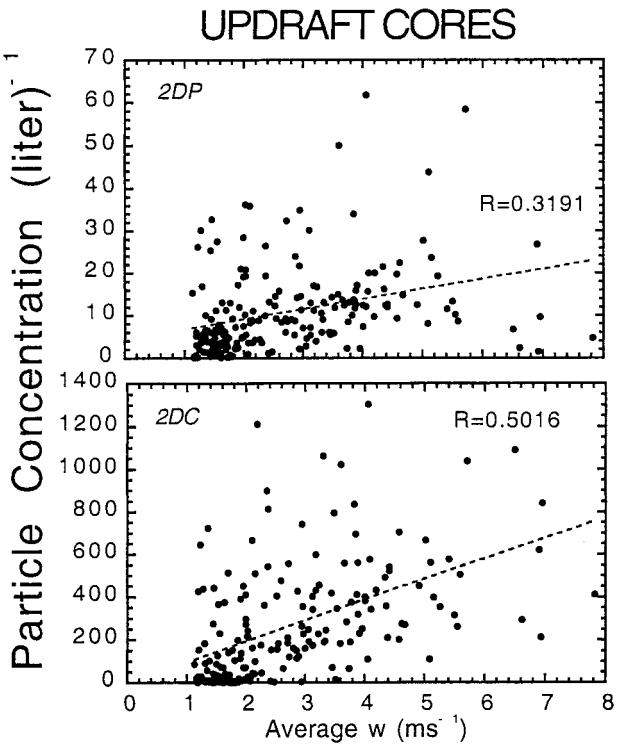

FIG. 7. For updraft cores sampled between 2.5 and 4.3 km; the relationship between average vertical velocity and average particle concentration, as expressed in number per liter, from the 2D-C (particle diameter d = 25–800 μm) and 2D-P (d = 200–6400 μm) probes.

tual temperature obtained assuming saturation. These cores were observed on five different days, mostly between 3.05 and 3.10 km above the surface. The liquid-water contents were estimated from 2D-C and 2D-P data by Wei et al. (1998).

According to the figure, neither the core-environment altitude differences nor water loading appear to alter the buoyancy of the downdraft cores significantly. The altitude effect (bottom of Fig. 9) is estimated by multiplying the difference between the average core altitude (z_c) and the environmental altitude (z_e) by the dry-adiabatic lapse rate (0.0098 K m^{-1}) to get the maximum reasonable effect. The deviation is positive if the airplane is at a lower altitude in the downdraft core ($z_c < z_e$). Altitude change affects the buoyancy by $\geq$0.2 K for only two downdraft cores. The middle frame in the figure corroborates the conclusion by Wei et al. (1998) made from examining all the COARE downdrafts with $w < -1$ m s^{-1}, namely, that water loading is not suf-

TABLE 4. Linear correlation coefficients of average and maximum 1-s T_v deviation with mean w, 1-s extreme value of w, w_{xtrm}, and apparent diameter D. Downdraft-core data are in parentheses. COARE data for 2.5–4.3 km only.

Parameter	Average θ_v deviation (K) EMEX (Lucas et al.)	Average T_v deviation (K) COARE	Maximum θ_v deviation (K) EMEX (Lucas et al.)	Maximum T_v deviation (K) COARE
Mean w	0.65	0.54	0.77	0.64
	(0.31)	(0.13)	(0.04)	(0.04)
w_{xtrm}	0.61	0.49	0.78	0.61
	(0.30)	(0.10)	(0.04)	(0.08)
D	0.23	0.00	0.35	0.10
	(0.12)	(0.07)	(0.03)	(0.14)

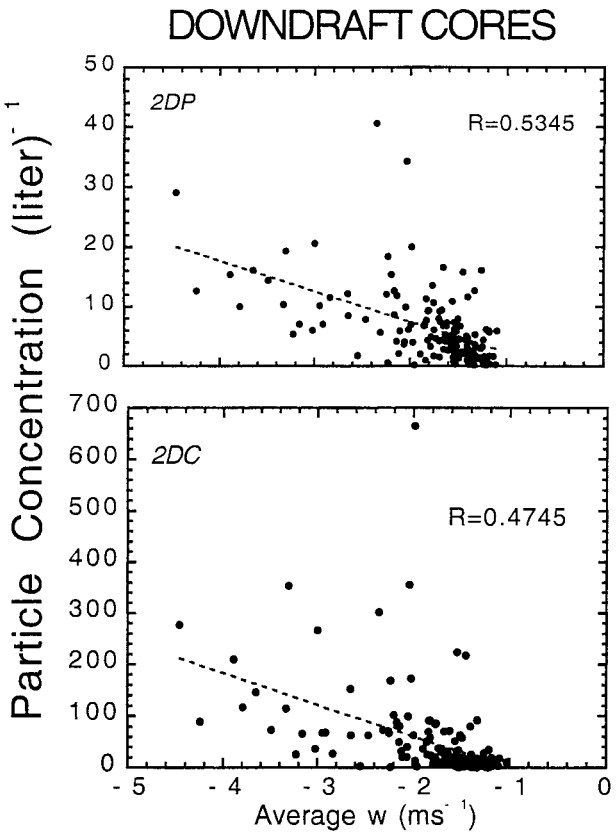

FIG. 8. As in Fig. 7 but for downdraft cores.

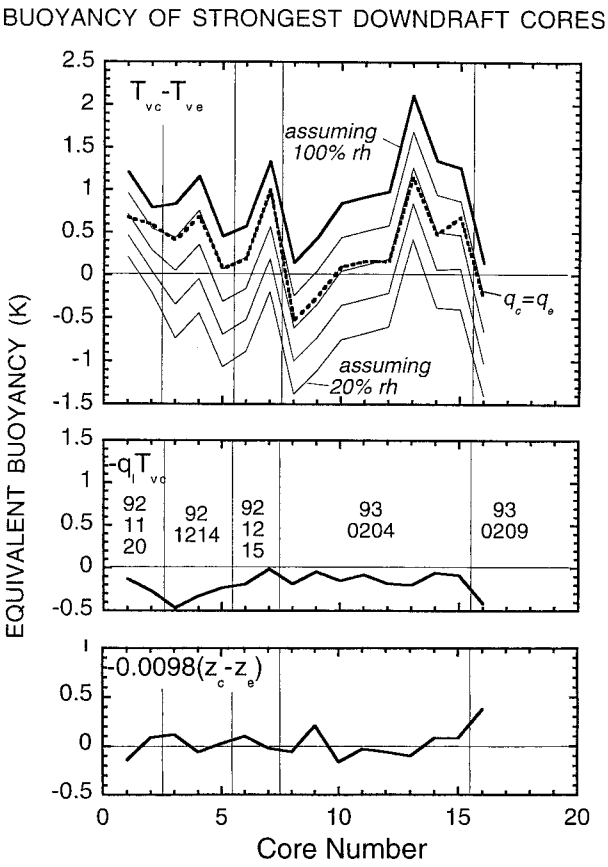

FIG. 9. Buoyancy components of the strongest downdraft cores. (top) Effects of assumed relative humidity in cores; (middle) effects of water loading; (bottom) effects of height difference between core and environment, using the dry-adiabatic lapse rate to convert altitude change to temperature change. Vertical lines separate the days (year-month-day) the cores were sampled. All cores sampled between 3.05 and 3.10 km (~700 mb) except for those of 19–20 November 1992, which were sampled at 4.28 km (~650 mb). In the top frame, thin solid lines represent virtual-temperature excess under assumption of 20%, 40%, 60%, and 80% core relative humidity; the thick solid line assumes 100%; and the thick dashed line represents both core temperature excess $T_c - T_e$ and core virtual-temperature excess $T_{vc} - T_{ve}$ assuming $q_c = q_e$. Water loading is computed from 2D-P and 2D-C microphysics data as in Wei et al. (1998).

ficient to remove their positive buoyancy found assuming saturation (heavy solid line, upper frame, Fig. 9).

However, the top frame shows that the relative humidity assumed in calculating T_v for the cores can have a significant effect. The heavy solid line is for T_v deviations computed assuming 100% relative humidity (RH) in the downdraft cores. However, saturation is by no means assured in downdraft cores, so we recalculate the core virtual temperature assuming core relative humidities (RH) of 80%, 60%, 40%, and 20%, using the relationship

$$T_v(\mathrm{RH}) = T_v(100\%) - 0.61(1 - 0.01\mathrm{RH}[\%])q_{\mathrm{sat}}T, \tag{1}$$

where q_{sat} (dimensionless) is the saturation mixing ratio at temperature T (thin lines in top frame of Fig. 9). Comparing the lines, a 20% decrease in relative humidity reduces the virtual-temperature excess by 0.2 K at 4.3 km and by 0.4 K at 3.1 km. Since (1) is linear, we can interpolate using the dashed curves in Fig. 9 to get the virtual-temperature excess for any hypothetical core relative humidity.

The heavy dashed line in the top panel, which represents the difference between core and environment temperatures, is approximately the same as the difference between the core and environmental virtual temperature, assuming that both have the same mixing ratio. For an environmental mixing ratio of q_e (gm gm^{-1}),

$$\begin{aligned} T_{vc} - T_{ve} &= T_c - T_e + 0.61q_e(T_c - T_e) \\ &\approx T_c - T_e, \end{aligned} \tag{2}$$

where the subscripts c and e represent core and environment, respectively.

We can use Fig. 9 to draw some important conclusions. First, several of the cores are probably positively buoyant. Assume that the cores have mixing ratios greater than or equal to their environment (heavy dashed curve). Comparing the three frames in the figure, 10 of the cores remain buoyant under this assumption. Com-

paring the dashed curve to the relative-humidity lines, this curve corresponds to a core and environment relative humidity of 60%–80%. This is consistent with typical relative humidities in the vicinity of deep tropical convection. For GATE, the composite soundings for fast- and slow-moving convective bands in Barnes and Sieckman (1984) show relative humidities below 600 mb of 80% for slow lines, and 60%–80% for fast lines. For COARE, LeMone et al. (1998) show relative humidities between 70% and 90% below 600 mb for their average deep-convective environmental sounding; one standard deviation lower is still greater than 60%.

To get the lowest reasonable core relative humidity, we apply parcel theory to the LeMone et al. (1998) proximity soundings. On 4 February, the day with the most warm cores, the lowest environmental relative humidity was reached, so we start with this day. Assume that the downdraft core with the highest virtual-temperature deviation (core 13) originated at 650 mb, the height of minimum Θ_e, where the environmental temperature and relative humidity are −9.5°C and 29%. In order for the parcel to have a 1 K T excess at 700 mb (Fig. 9), the parcel temperature would have to reach 11.6°C (T_e = 10.6 C), meaning about 1 g of moisture would have to evaporate. Adding this to the original parcel mixing ratio (2.8 g kg^{-1}) yields a parcel (and core) relative humidity of around 30%. This is almost certainly lower than the actual core relative humidity since entrainment would have raised the relative humidity (environmental RH rises rapidly from 29% at 650 mb to 48% at 700 mb). Similar calculations produce a minimum core relative humidity of ~65% on 14 December (cores 3–5) and 50%–55% on 15 December (cores 6 and 7). The cores of 20 November are at the height of minimum Θ_e, so penetrative downdrafts are unlikely. *Five cores—cores 1, 2, 4, 7, and 13—retain positive buoyancies even assuming these low core relative humidities.*

Second, the use of the 100% RH assumption probably conspired with the difference in the two temperature instruments to give higher-temperature downdraft cores in COARE. Jorgensen and LeMone (1989) suggested that raindrops would assume the wet-bulb temperature, which they estimated to be ~1 K lower than the air. Consider a hypothetical Barnes radiometer that senses only drop temperature. Then, if the Ophir and hypothetical radiometers were looking at the same target, the hypothetical radiometer would see a temperature 1 K lower than the Ophir. At 700 mb and a typical temperature of 283 K, the hypothetical radiometer would read 282 K, whose water vapor saturation value is 87% that at 283 K. From Fig. 9, the saturation assumption would account for an additional 13%/20% × 0.4 K = 0.3 K cooling in apparent virtual temperature, and the hypothetical radiometer's virtual temperature reading would be 1.3 K lower than the Ophir value. A calculation that more accurately represents the mixture of air and drops

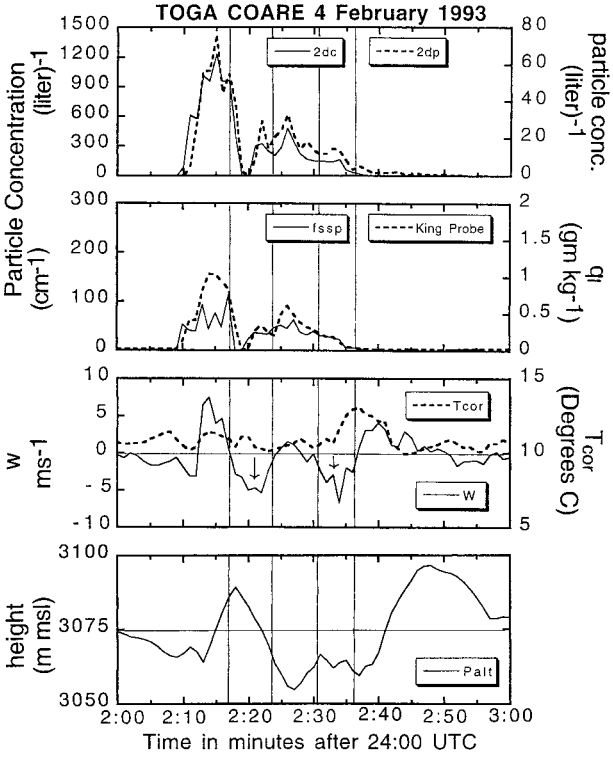

FIG. 10. As in Fig. 3 but only downdraft cores 12 and 13 of Fig. 9 are outlined. These cores were sampled in relatively isolated cumulus congestus.

seen by the Barnes instrument would reduce this number to a more reasonable value.

Finally, the positive temperature deviations (the $q_c = q_e$ curve) and the low liquid-water contents in Fig. 9 suggest that at least portions of some downdraft cores are subsaturated. A look at the individual time series confirms this fact. For example, the FSSP particle count, which reflects mainly cloud droplets, drops to near zero for core 10, shown in Fig. 3. Likewise, Fig. 10 shows two downdraft cores (cores 12 and 13) with regions of near-zero FSSP counts, and cores 9 and 15 (not shown) have regions with FSSP counts <6 cm^{-3}. In contrast, the sampled portion of the most negatively buoyant core in Fig. 9 (core 16) has FSSP counts >20 cm^{-3} throughout (Fig. 11).

Although we have not calculated water loading or minimum possible buoyancies for all 147 downdraft cores analyzed, we can easily compare the distributions of T_v deviations obtained from the core-saturation assumption and the ($q_c = q_e$) assumption. Figure 12 compares the distribution of average temperature deviations for downdraft cores to the distribution of average T_v deviations. For the T_v-deviation distribution, use of the saturation assumption to obtain T_{vc} leads to 70% of the downdraft cores with positive T_v deviations. For the T-deviation distribution, which from the foregoing is equivalent to the T_v distribution assuming $q_c = q_e$, 45%

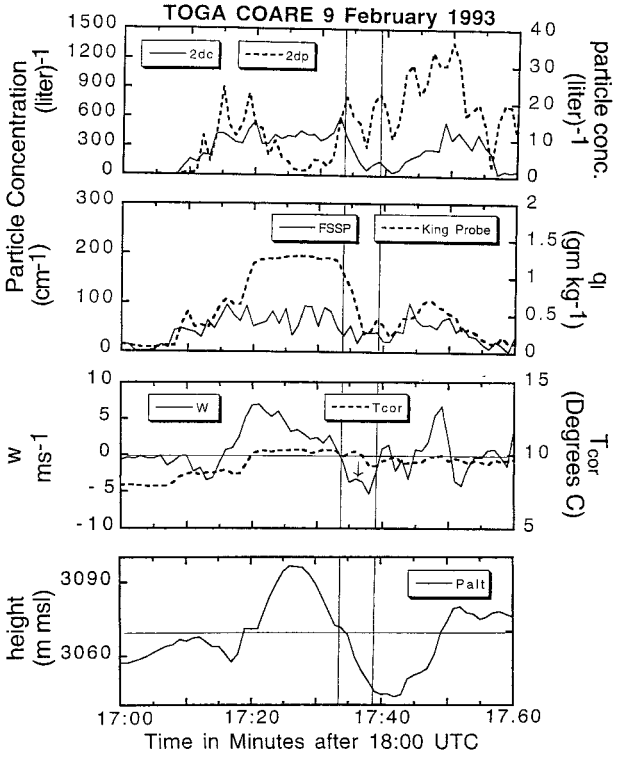

FIG. 11. As in Fig. 10 but for core 16 of Fig. 9. This core was sampled in a well-developed convective band, observed on 9 February 1993.

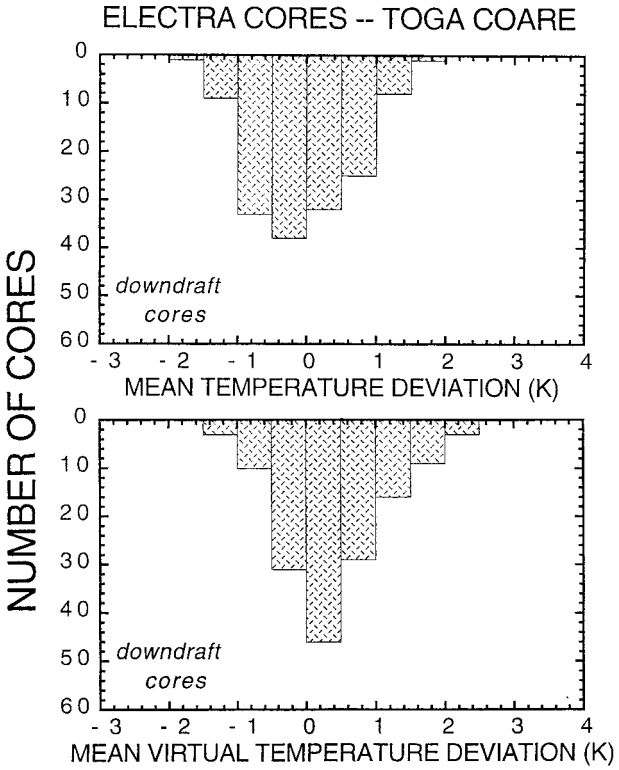

FIG. 12. Distributions of mean temperature deviation (top) and mean virtual temperature deviation (bottom) for downdraft cores sampled between 2.5 and 4.3 km.

of the downdraft cores have positive T_v deviations—still a significant percentage.

Downdraft-event data from a numerical simulation of GATE cloud systems using the Clark–Hall cloud-resolving model (Clark et al. 1996; Grabowski et al. 1998) are consistent with our impressions that (a) relative humidities in downdraft cores are often less than 100% and (b) that water loading does not eliminate buoyant cores. W. W. Grabowski (1998, personal communication) provided us a collection of 379 downdraft events, sampled at 20-min intervals at about 3 km msl for the period 1500–2100 UTC 2 September 1974 (GATE day 245). Grid boxes (2×2 km) with vertical velocities less than -1 m s^{-1} and rain or cloud water were considered downdraft events. The model was configured to simulate the behavior of GATE convection over a 400-$\times$ 400-km area over seven days, using horizontally averaged vertical profiles and a constant sea surface temperature as input. The model has 42 levels in the vertical, with vertical grid spacing increasing linearly from 100 m near the surface to 1200 m at the model top. The model uses a Kessler (1969) warm rain parameterization and the Koenig and Murray (1976) two-class ice parameterization. It keeps track of rain water, cloud water, and two types of ice particles, low density and high density.

Relative humidities for the simulated downdraft events range from 69% to 100% (only 9 are saturated), with a median value of 90%. Of the 379 events, 171 (45%) are warmer than the domain average; of these, 108 (63%) have relative humidities lower than the domain average value of 88%. The events with the lower relative humidities tend to have larger negative vertical velocities. Assuming saturation for the model downdraft events for comparison with Fig. 5 and Table 3 raises the equivalent buoyancy (excluding water loading) by 0.13 K, from -0.05 to $+0.08$ K.

As in the case for all the COARE downdraft cores (Wei et al. 1998) and for the downdraft cores of Fig. 9, water loading for the model downdraft events was surprisingly small. The average equivalent buoyancy for the water-loaded downdraft events is -0.15 K, only 0.1 K lower than the average accounting for thermal and water vapor effects only. Fully 38% of the downdraft events are still positively buoyant when water loading is included along with water vapor and thermal effects.

Although the microphysics parameterizations in the model are highly idealized, and although there is not a direct correspondence between the observed cores and the modeled events, both the data and the model results suggest that in determinations of downdraft-core buoyancy *subsaturation cannot be neglected and water loading is surprisingly small.*

Thus, positively buoyant downdrafts are probably

common. They could be overshooting downdrafts initially driven by negative buoyancy, as illustrated by the one-dimensional model of Srivastiva (1987). They could be the downward-moving portions of gravity waves, suggested by Yang and Houze (1995) to occur in squall lines. Vertical pressure forces driven by the surrounding shear and buoyancy field probably play an important role in determining the frequency of thermally buoyant downdraft cores. There is ample modeling (e.g., Rotunno and Klemp 1982) and observational evidence (e.g., Marwitz 1972; Marwitz et al. 1972; LeMone et al. 1988; Barnes 1995) that these forces can be significant (e.g., Rotunno and Klemp 1982), especially for updrafts. More recently, Trier et al. (1997) showed in a simulation of the TOGA COARE 22 February case that updrafts were sensitive to the vertical pressure gradient, a sensitivity that is supported by observations (Jorgensen et al. 1997) of the variability of structure across this convective system.

Based on a numerical simulation of the 22 February 1993 TOGA COARE squall line, Trier et al. (1997) and Trier (1997) suggest that downdraft-core temperature is a function of the three-dimensional convective environment in which the core occurs. Trier (1997) found that the warmest downdrafts were associated with more isolated convection. By doing trajectory analyses in two parts of the system, he found that the trajectory in the isolated convection passed through less continuous rain that was less heavy, and remained relatively warm and subsaturated as it sank toward the surface. In contrast, the downdraft air descending in the part of the system more organized on the mesoscale encountered more continuous, heavy rain, warmed more slowly, and arrived at the surface cooler and moister but with the same equivalent potential temperature as the warm downdraft air. In many cases, these downdrafts would initially sink due to water loading rather than cool temperatures.

Although the details are different for the cores of Fig. 9, a similar tendency is apparent: many of the warm cores occur in isolated clouds. Examining videos from the flights shows that half the cores of Fig. 9, those of 4 February, are associated with isolated cumulus towers just ahead of a convective band. However, other warm cores, for example, cores 1, 2, and 7, are embedded in widespread convection.

5. Conclusions

The convective updraft and downdraft cores of TOGA COARE have similar diameters and strengths to cores observed elsewhere over the tropical oceans and are weaker and smaller in diameter than their continental counterparts. As in TAMEX (Jorgensen and LeMone 1989) and EMEX (Lucas et al. 1994), the downdraft cores sampled include a surprising number of individuals with virtual temperatures higher than the environment. It is particularly surprising that the COARE downdraft cores have an average virtual-temperature excess equal to that of the updraft cores. The COARE downdraft cores also tend to have T_v excesses larger than those observed in TAMEX and EMEX. Thus we decided to study 16 of the most intense downdraft cores, all of which had virtual temperatures warmer than their environments, to examine the cause, physical or otherwise, of the warm downdraft cores.

An examination of the water loading, the height difference between the environment and the core, and the assumption of 100% relative humidity for the 16 cores suggests that the 100% relative humidity assumption for downdraft cores exaggerates both the number of cores with positive T_v deviations and the buoyancy of the cores. Recalculating the buoyancies assuming an 80% relative humidity reduces the T_v excess by 0.4 K at 3 km—a significant amount. Subsaturated downdraft cores are not surprising (e.g., Srivastiva 1987): they were recognized as a possibility in Jorgensen and LeMone (1989), who used the 100% assumption for lack of an obvious alternative. Downdraft events extracted from the Grabowski et al. (1998) simulation of GATE day 245 typically have relative humidities less than 100% (median value 90%). Given unsaturated downdrafts, the Ophir radiometer's sensitivity to air temperature as opposed to the modified Barnes radiometer sensitivity to air and raindrops could account for the COARE downdraft cores having higher T_v excesses than those in TAMEX and EMEX.

However, some of the COARE downdraft cores, possibly even a significant fraction, are probably positively buoyant. Ten of the 16 downdraft cores in Fig. 9 are positively buoyant if we assume core mixing ratios equal to environmental values. Five remain buoyant even with our estimates of minimum possible core relative humidities. Over a third of the downdraft events in the Grabowski et al. (1998) GATE simulation sample were buoyant relative to the domain average. The positively buoyant downdraft cores could be simply overshooting downdrafts or the downward-moving parts of gravity waves, or caused by more complex interplay of the forces generated by the surrounding three-dimensional convection and its immediate environment. In Fig. 9, as in the simulation of the 22 February TOGA COARE squall line system by Trier (1997), warm downdraft cores are often associated with more isolated convection.

We conclude that more work needs to be done to understand the behavior of downdraft cores. Numerical simulations have and will help greatly, but observations of relative humidity are crucial to a better understanding of convective downdrafts.

Acknowledgments. This work was dependent on many other people. In particular, we wish to acknowledge the flight, technical, and scientific crews of the NCAR Electra, and the many flight scientists, in particular Gary Barnes, Alan Blyth, David Raymond, and Robert Grossman. NCAR's Atmospheric Technology Division did the

initial processing of the Electra data in a timely manner, and David Raymond processed the Electra data further. Dingying Wei acknowledges the help of her advisor, Alan Blyth, and David Raymond. We had many useful discussions with Al Cooper and Paul Lawson. Wojciech Grabowski provided model data for the core analysis. Edward Zipser provided advice and encouragement throughout the course of the work. Garpee Barleszi offered acerbic but sometimes useful remarks and advised us on creative financing. The farsighted decision of NOAA and NSF sponsors to encourage student participation in TOGA COARE enabled Igau to participate in the field program. Igau received support through NSF Grants ATM 91-10479, the NCAR Mesoscale and Microscale visitors' program, and NCAR's Advanced Study Program. Partial support for LeMone was from NSF Grant ATM9215508. Wei was supported by NSF Grant ATM-9413289 and TOGA COARE Grant ATM-9112043.

REFERENCES

Albrecht, B. A., S. K. Cox, and W. H. Schubert, 1979: Radiometric measurements of in-cloud temperature fluctuations. *J. Appl. Meteor.,* **18,** 1066–1071.

Barnes, G. M., 1995: Updraft evolution: A perspective from cloud base. *Mon. Wea. Rev.*, **123,** 2693–2715.

——, and K. Sieckman, 1984: The environment of fast- and slow-moving tropical mesoscale convective cloud lines. *Mon. Wea. Rev.,* **112,** 1782–1794.

Blyth, A. M., W. A. Cooper, and J. B. Jensen, 1988: A study of the source of entrained air in Montana cumuli. *J. Atmos. Sci.,* **45,** 3944–3964.

Byers, H. R., and R. R. Braham, 1949: The Thunderstorm Project. U.S. Weather Bureau, U.S. Dept. of Commerce Tech. Rep., 298 pp. [NTIS PB234515.]

Clark, T. L., W. D. Hall, and J. L. Coen, 1996: Source code documentation for the Clark–Hall cloud-scale model: Code version G3CH01. NCAR Tech. Note NCAR/TN-426+STR, 137 pp. [Available from NCAR Information Service, P.O. Box 3000, Boulder, CO 80307.]

Cooper, W. A., 1987: The Ophir Radiometric Thermometer: Preliminary Evaluation. NCAR Tech. Note NCAR/TN-292+STR, 54 pp.

Grabowski, W. W., X. Wu, M. W. Moncrieff, and W. D. Hall, 1998: Cloud-resolving modeling of tropical cloud systems during Phase III of GATE. Part II: Effects of resolution and the third spatial dimension. *J. Atmos. Sci.,* **55,** 3264–3282.

Heymsfield, A. J., and M. R. Hjelmfelt, 1981: Dynamical and microphysical observations in two Oklahoma squall lines. Part II: In-situ measurements. Preprints, *20th Conf. on Radar Meteorology,* Boston, MA, Amer. Meteor. Soc., 60–65.

——, J. E. Dye, and C. J. Biter, 1979: Overestimates of entrainment from wetting of the aircraft temperature sensors in cloud. *J. Appl. Meteor.,* **18,** 92–95.

Jorgensen, D. P., and M. A. LeMone, 1989: Vertical velocity characteristics of oceanic convection. *J. Atmos. Sci.,* **46,** 621–640.

——, E. J. Zipser, and M. A. LeMone, 1985: Vertical motions in intense hurricanes. *J. Atmos. Sci.,* **42,** 839–856.

——, M. A. LeMone, and S. B. Trier, 1997: Structure and evolution of the 22 February 1993 TOGA COARE squall line: Aircraft observations of structure, circulation, and surface energy fluxes. *J. Atmos. Sci.,* **54,** 1961–1985.

Kessler, E., 1969: *On the Distribution and Continuity of Water Substance in Atmospheric Circulations. Meteor. Monogr.,* No. 32, Amer. Meteor. Soc., 84 pp.

Koenig, L. R., and F. W. Murray, 1976: Ice-bearing cumulus cloud evolution: Numerical simulation and generation comparison against observations. *J. Appl. Meteor.,* **15,** 747–762.

Lawson, R. P., and A. Rodi, 1987: Airborne tests of sensor wetting in a reverse-flow temperature probe. *Extended Abstracts, Sixth Symp. on Meteorological Observations and Instrumentation,* New Orleans, LA, Amer. Meteor. Soc., 253–256.

——, and W. A. Cooper, 1990: Performance of some airborne thermometers in cloud. *J. Atmos. Oceanic Technol.,* **7,** 480–494.

LeMone, M. A., 1980: On the difficulty of measuring temperature and humidity in cloud: Comments on ''shallow convection on day 261 of GATE.'' *Mon. Wea. Rev.,* **108,** 1702–1705.

——, and E. J. Zipser, 1980: Cumulonimbus vertical velocity events in GATE. Part I: Diameter, intensity, and mass flux. *J. Atmos. Sci.,* **37,** 2444–2457.

——, G. M. Barnes, J. C. Fankhauser, and L. F. Tarleton, 1988: Perturbation pressure fields measured by aircraft around the cloud-base updraft of deep convective clouds. *Mon. Wea. Rev.,* **116,** 313–327.

——, E. J. Zipser, and S. B. Trier, 1998: The role of environmental shear and thermodynamic conditions in determining the structure and evolution of mesoscale convective systems during TOGA COARE. *J. Atmos. Sci.,* **55,** 3493–3518.

Lenschow, D. H., 1972: The measurement of air velocity and temperature using the NCAR Buffalo aircraft Measuring System. NCAR Tech. Note NCAR-TN-EDD-74, 39 pp.

——, and W. T. Pennell, 1974: On the measurement of in-cloud and wet-bulb temperature from an aircraft. *Mon. Wea. Rev.,* **102,** 447–454.

Lucas, C., E. J. Zipser, and M. A. LeMone, 1994: Vertical velocity in oceanic convection off tropical Australia. *J. Atmos. Sci.,* **51,** 3183–3193.

Marwitz, J. D., 1973: Trajectories within the weak echo region of hailstorms. *J. Appl. Meteor.,* **12,** 1174–1182.

——, A. H. Auer Jr., and D. L. Veal, 1972: Locating the organized updraft on severe thunderstorms. *J. Appl. Meteor.,* **11,** 236–238.

Musil, D. J., A. J. Heymsfield, and P. L. Smith, 1986: Microphysical characteristics of a well-developed weak echo region in a High Plains supercell thunderstorm. *J. Climate Appl. Meteor.,* **25,** 1037–1051.

Rotunno, R., and J. B. Klemp, 1982: The influence of shear-induced pressure on thunderstorm motion. *Mon. Wea. Rev.,* **110,** 136–151.

Srivastiva, R. C., 1987: A model of intense downdrafts driven by the melting and evaporation of precipitation. *J. Atmos. Sci.,* **44,** 1752–1773.

Trier, S. B., 1997: Multiscale analysis of a simulated oceanic mesoscale convective system and its environmental impact. Ph.D. dissertation, Colorado State University, 241 pp. [Available from University Microfilm, 305 N. Zeeb Rd., Ann Arbor, MI 48106.]

——, W. C. Skamarock, and M. A. LeMone, 1997: Structure and evolution of the 22 February squall line: Organization mechanisms inferred from numerical simulation. *J. Atmos. Sci.,* **54,** 386–407.

Webster, P. J., and R. Lukas, 1992: TOGA COARE: The Coupled Ocean–Atmosphere Response Experiment. *Bull. Amer. Meteor. Soc.,* **73,** 1377–1416.

Wei, D., A. M. Blyth, and D. J. Raymond, 1998: Buoyancy of convective clouds in TOGA COARE. *J. Atmos. Sci.,* **55,** 3381–3391.

Yang, M.-J., and R. A. Houze Jr., 1995: Multicell squall line structure as a manifestation of vertical trapped gravity waves. *Mon. Wea. Rev.,* **123,** 641–661.

Zipser, E. J., and M. A. LeMone, 1980: Cumulonimbus vertical velocity events in GATE. Part II: Synthesis and model core structure. *J. Atmos. Sci.,* **37,** 2458–2469.

——, R. J. Meitin, and M. A. LeMone, 1981: Mesoscale motion fields associated with a slowly moving GATE convective band. *J. Atmos. Sci.,* **38,** 1725–1750.